LA-UR- 08-4754

Approved for public release; distribution is unlimited.

Title:	SURFACE POLARITY OF β-HMX CRYSTAL AND THE RELATED ADHESIVE FORCES WITH ESTANE BINDER
Author(s):	Lu Yang, David E. Hanson
Intended for:	Journal of Chemical Physics

Los Alamos
NATIONAL LABORATORY
EST. 1943

Form 836 (7/06)

Surface polarity of β-HMX crystal and the related adhesive forces with Estane binder

Lu Yang* and David E. Hanson

Theoretical Chemistry & Molecular Physics (T-12) Group

Los Alamos National Laboratory, Los Alamos, New Mexico, NM 87545

(Dated: July 14, 2008)

Abstract

Here we present the results on the study of surface properties of β-HMX crystal utlizing molecular simulations. The surface polarity of three principal crystal surfaces are investigated by measuring the water contact angles. The calculated contact angles agree excellently with the values measured by experiment and show that the surface polarity of three crystal surfaces are different. The free energies and forces of detaching an Estane chain with and without nitroplasticizer from the three principal crystal surfaces were calculated using umbrella sampling technique. We find that the detaching free energy/force increases with the increasing HMX surface polarity. In addition, our results also show that nitroplasticizer plays an important role in the adhesion forces between Estane and HMX surfaces.

PACS numbers:

*Electronic address: yangl@lanl.gov

I. INTRODUCTION

HMX (octahydro-1,3,5,7-tetranitro-1,3,5,7-tetrazine) based polymer bonded explosives (PBXs) are widely used in both civil and military applications for their high energy density, high melting point, and relatively low sensitivity to inadvertent detonation. In addition to the energetic high explosive materials HMX, the design of PBXs also require the diligent choice of an appropriate binder which holds the HMX grains together. For maximum explosive performance, the level of binder is normally restricted to a relatively low percentage (4-8 vol%) [1]. Two well known examples are LX-14, which comprises 95.5% HMX and 4.5% Estane, and PBX9501, which comprises 95% HMX and 5% Estane/nitroplasticizer (1:1) [2].

Despite its low content, studies have shown that the binder has a significant effect on the properties and response of PBX composites [2]. Both the mechanical properties and sensitivity of a composite depend on the strength of interfacial forces, or in other words, adhesion between HMX surfaces and polymer binder. There is evidence in the literature that failure in tension of PBX materials begins with adhesive failure at multiple sites between the largest crystals of HMX and the polymeric binder system. These sites can propagate and link up, leading to global failure of the sample under consideration. The presence of defects, such as voids or cracks, can greatly increase the sensitivity of PBX materials because they are potential hot spots where chemical reactions are likely to happen and also because they increase the specific area available for combustion. In addition, the conversion of undesirable impact sensitive δ-HMX to insensitive β-HMX is also facilitated by the adhesion between HMX crystals and binder [3, 4]. Experiment has shown that the aged binder materials which lose adhesion to the crystalline HMX retard δ-to-β reconversion [5]. For PBXs as well as propellants, one of the greatest concern is the possibility of accidental initiation during manufacture, transportation or handling. Adhesion between HMX crystal surface and polymer binder, which controls the mechanical strength and sensitivity, therefore has a very important role in PBX materials.

Adhesion arises from the molecular interactions at the interface between the crystal surfaces of HMX and the polymer binder. At present little is known about the details of the surface properties of HMX crystal and their interactions with polymer binder. A better understanding of the HMX-binder interficial structure and interactions permits the selection/design of polymer binder that promote stronger interactions between the srystalline materials and the polymer binder, which might enhance the stability of PBX. In particular, Yee *et. al*, has shown that the properties of

different crystal surface of HMX are different. This implies that polymer binders could be selected/designed that bind preferentially to specific crystal faces.

It is, therefore of obvious interest to characterize the surface properties of β-HMX surface and measure the free energy and force which are required to cause adhesive failure between HMX and the polymer binder. In this paper we demonstrate, for the first time, the use of Molecular Dynamics simulations to characterize the polarity of β-phase HMX surfaces using water contacting angle as the indicator. Results from theoretical calculations have excellent agreement with previous experimental measurement. Specifically, we investigate the molecular interactions among the different surfaces of β-HMX, polymer binder and nitroplasticizer (NP). The free energy/force required to detach the polymer binder from HMX different surfaces with and without NP is calculated utilizing umbrella sampling techniques. We find that the polarity of the HMX crystal surfaces dominates the corresponding force for detachment. In addition, these simulations provide insights to the structure-performance relationships at the HMX-binder interface, which, inturn may help design better and more efficient PBX.

II. METHODOLOGY

Crystalline HMX exists in four different polymorphs, namely, α, β, γ, and δ forms, with β-HMX the most stable structure at room temperature and pressure. Therefore, β-HMX was selected in this study to construct the HMX crystal surfaces. A series of MD simulations of water droplets and Estane chain with and without nitroplasticizer on the three principal surfaces of β-HMX crystal were performed. We simulated water droplets and Estane chain on the HMX crystal 011, 010, and 110 surfaces which were extracted from the crystal structure of β-HMX utilizing software Mercury [6]. The surface area of HMX ranged from 60 $\times$ 60 Å to 200 $\times$ 200 Å depending on the size of water droplets and the length of Estane chain, and the box size in the direction perpendicular to the HMX surface was increased by at least 50 Å to effectively remove the periodic image effect. The HMX surfaces consisted one or two staggered sheet depending on the surface structure. Additional sheets of HMX were omitted because they are not expected to have a significant influence on the droplets of water and the Estane chain. In all of the simulations, the HMX crystal surfaces were fixed at their respective initial positions and represent an inert wall. Simulation parameters for HMX, Estane, and nitroplasticizer were taken from literature [7–10], while water molecules were represented by SPC/E water model [11]. Particle mesh Ewald summation

[12] was used to calculate electrostatic interactions with a grid spacing of 1.0 Å . Lennard-Jones interactions in the systems was calculated using Lorentz-Berthelot mixing rules and a cutoff radius of 10 Å was employed. All the simulations were performed under NVT ensemble using AMBER 9. The SHAKE algorithm [13] was used to constrain the bonds involve hydrogen so that it was possible to use a time step of 2 fs. In the following, more MD simulation detail is described along with the procedure on how water contact angle, free energy and force of Estane detachment were extracted from the simulations.

A. Water contact angle

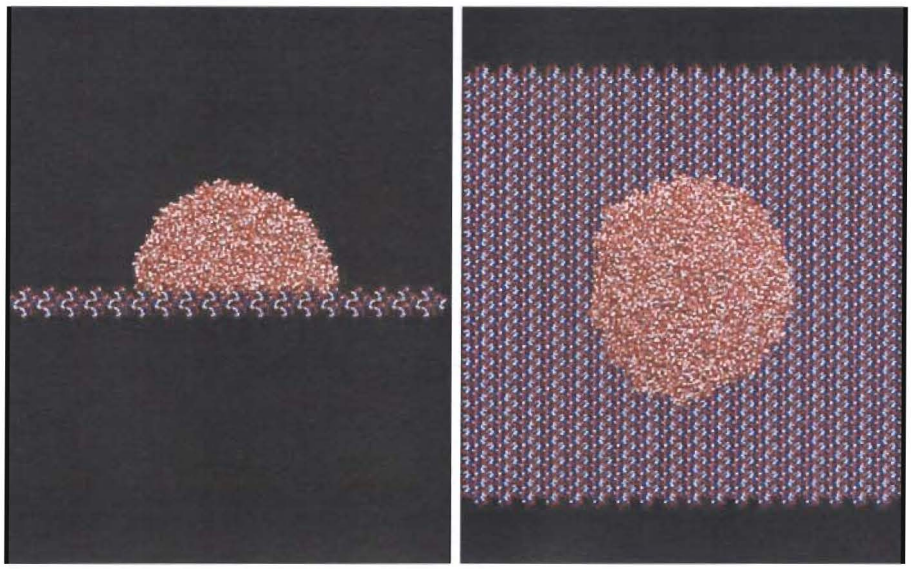

FIG. 1: Side view (left) and top view (right) of a water droplet on the surface of HMX 010. Water molecules are shown in red (oxygen) and white (hydrogen) spheres while HMX molecules are shown in sticks with oxygen in red, hydrogen in white, carbon in cyan, and nitrogen in blue.

Randomly packed semi-spherical water droplets with realistic density were added on the top of HMX 011, 010, and 110 surfaces. To investigate the dependence of the water contact angle on the size of the water droplet, simulations with 2000, 4000, and 8000 water molecules were performed. All nine simulations were carried out for 2 ns with the first nanosecond as the equilibration time. In the first half nanosecond of equilibration time, the system was coupled to a Berendsen thermostat [14] at a temperature of 250 K, whereas in the second half of the equilibration time and in the production run the temperature was coupled at 300 K. Samples of trajectory were stored every

1 ps for further analysis. A snapshot of the water droplet on the HMX 010 surface is shown in Figure 1.

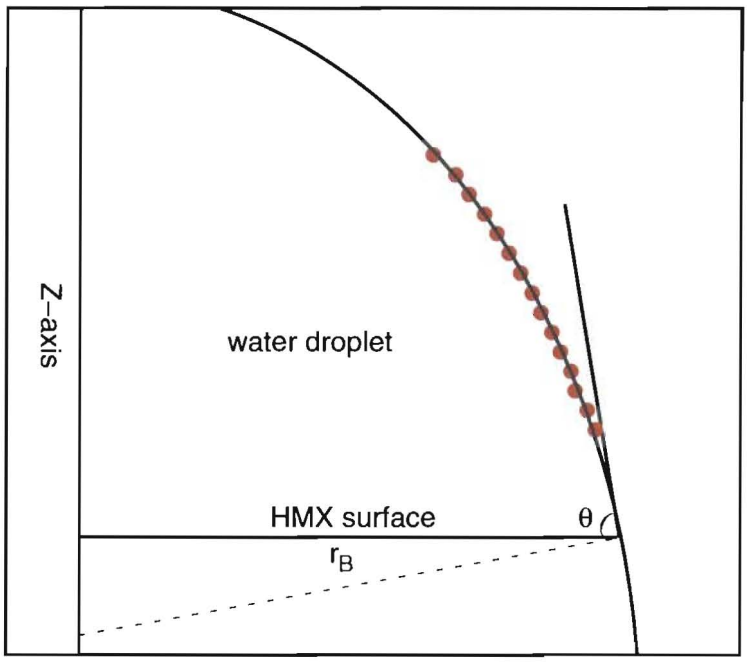

FIG. 2: Contact angle θ measured by fitting a circle with center of (0,B) and radius of A to the points at water-vaccum interface (dots). Dots on the top and near the interface region are excluded in the fitting procedure. The droplet has a base radius r_B.

We follow a precedure similar to that developed by werder et. al. [15] and Giovambattista at. el. [16]. to calculate the water contact angle. We first define a reference axis (Z) which is perpendicular to the HMX surface and passes through the center of mass of the water droplet. We then divide the water droplet into slabs of height 1 Å parallel to the HMX surface. In each slab, we introduce cylindrical bins centered at z-axis with the surface area of $\delta A = 30\mathring{A}^2$. The radius of each bin are therefore determined by $r_i = \sqrt{i\delta A/\pi}$ for i=1,...,N_{bin}. We then calculate the density of water molecules in all the bins for each slab to obtain the horizontal density profiles as a function of bin radius. We define the water-vaccum interface from these density profiles as a location where the density falls below $0.5g/cm^3$. Finally, we fit the interface points with a circular function $r_{droplet}(z) = \sqrt{A^2 - (z-B)^2}$ (A, B are constant) and determine the contact angle at the point where the fitted circle and the HMX surface meet. Density profile of HMX were used to locate the HMX surface. In the fitting procedure, data points within $4 \sim 6$ Å of the HMX surface and in the cap region were not taken into account to avoid the influence of density fluctuations.

Figure 2 illustrates the typical procedure of water contact angle measurement.

To compare the microscopic water contact angle calculated from molecular dynamics simulations with the macroscopic angle measured from experiment, the effect of line tension τ has to be taken into account. The deviating of microscopic contact angle from the macroscopic angle θ_∞ due to the effect of line tension τ is described by the modified Young's equation [15, 17],

$$cos\theta = cos\theta_\infty - \frac{\tau}{\gamma_{LV}} \frac{1}{r_B} \tag{1}$$

where τ is the line tension, γ_{LV} is the surface tension for liquid and vapor phases, and $1/r_B$ is the droplet base curvature. According to eq 1, the macroscopic contact angle θ_∞ of water droplet on HMX surfaces can be extrapolated from the calculated microscopic contact angle θ and the contact line curvature $1/r_B$ for water droplets of different sizes.

B. Detachment of an estane chain from HMX surfaces

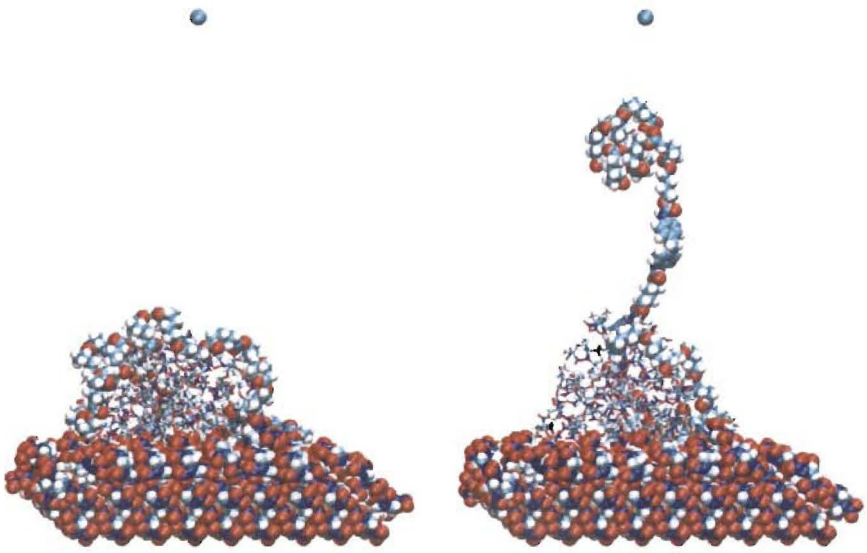

FIG. 3: Left: The droplet of Estane chain equilibrated with nitroplasticizer on the 010 surface of HMX crystal. The dummy atom used for umbrella sampling is also shown above the HMX and Estane droplet. Right: A snapshot of the system with the Estane chain pulled toward the dummy atom. Estane chain, HMX surface, and dummy atom are shown in spheres and the nitroplasticizer (BDNPA/BDNPF) are shown in sticks. Oxygen atoms are displayed in red, hydrogen atoms are displayed in white, nitrogen atoms are displayed in blue while carbon atoms are displayed in cyan.

To obtain the free energy and force required to cause adhesive failure between HMX surfaces and the binder (Estane and nitroplasticizer), we first constructed an Estane oligomer containing 4 poly(tetramethylene diphenylmethane-urethane)(PTDU) rigid segments in the middle and 5 poly(butylene adipate) (PBA) soft segments at two ends, respectively. (This Estane chain has $\sim$ 40 wt % hard segment, which is within the range of real materials (23%) since during processing and manufacturing, the hard segment might segregate at the polymer-HMX interface, leading to higher concentration of hard segment.) This Estane chain was then equilibrated with 30 nitroplasticizer molecules [50/50-wt% eutectic of bis(2,2-dinitropropyl) formal/acetal] for 6 ns to form a droplet of Estane binder. It is generally believed that the hard segments tend to clump together and bind the HMX surfaces, giving the polymer its strength, and the soft segments providing its flexibility. Therefore, we put the equilibrated binder droplet on the surfaces of HMX crystal with the hard segments closely contact with HMX, followed by 6 ns of equilibration to establish adhesion. A snapshot of the equilibrated Estane binder droplet on HMX surface 010 is shown in Figure 3 (Left).

Preliminary simulation results have shown that the rigid segment binds the HMX stronger than that of soft segment, therefore, we only focus on detaching the rigid segment from HMX in this study. Umbrella Sampling method is used to obtain the free energy and force of detaching Estane chain from the HMX surfaces. Details of this technique have been reported in elsewhere [18, 19]. Here we only present the basic idea. The key of umbrella sampling technique is using a harmonic spring to bias the sampling of low probability events, such as the detached Estane from the HMX surfaces in this study. To achieve this goal, we added a dummy atom 100 Å above the HMX surface and the position of the dummy atom is fixed. The harmonic spring connects the dummy atom and the first atom of the hard segment. The energy of the harmonic spring was $U^{'}(r) = k_r(r - r_0)^2$ where k_r is the force constant, r is the instantaneous distance between the dummy atom and the first atom of Estane hard segment, and r_0 is the predefined distance that minimizes the biasing potential $U^{'}(r)$. In this study, we performed simulations with $k_r = 0.5\ kcal/mol/\mathring{A}^2$ and r_0 ranges from 6 to 58 Å with a length step of 2 Å . These simulations provided us with well overlapped biased probability distributions $P^{'}(r)$ which are essential to extract the free energy profile on extension. Weighted Histogram Analysis Method (WHAM) [18? , 19] is used to remove the effect of the bias potential $U^{'}(r)$ and calculate the free energy of detaching the Estane hard segment from HMX

surfaces, as described in Equation 2

$$PMF(r) = -KT * lnP^{'}(r) - U^{'}(r) + F \tag{2}$$

where F is an undetermined but irrelevant offsets which depends on $U^{'}(r)$. The differentiation of PMF(r) with respect to chain extension *r* provides the restoring force. All of these simulations are performed for 3 ns at 300K using Berendsen thermostat. To investigate the effect of nitroplasticizer on the adhesion between Estane and HMX surfaces, the same procedure has been applied to the identical system with nitroplasticizer removed.

III. RESULTS AND DISCUSSIONS

A. Water contact angle

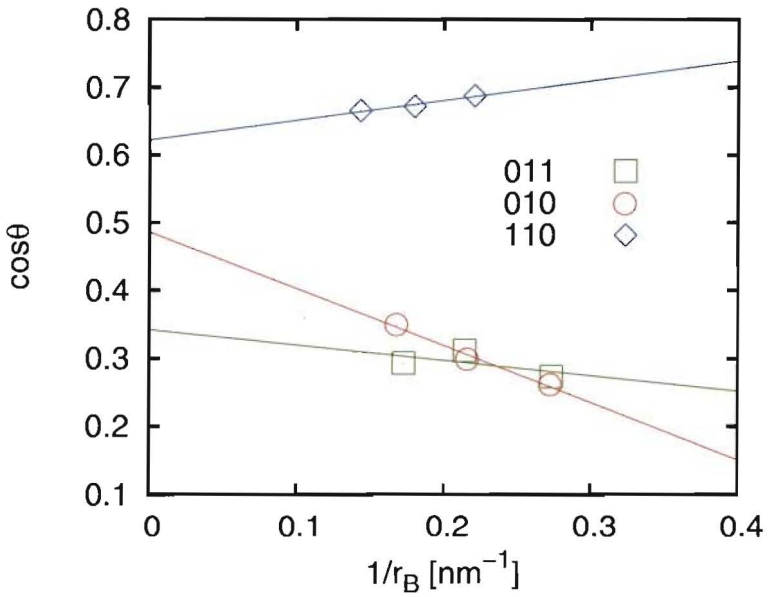

FIG. 4: Cosine of water contact angle θ calculated from MD simulations as a function of the droplet base curvature $1/r_B$ on the HMX 011 (square), 010 (cycle), and 110 (diamond) surfaces. The lines indicate the linear least-square fitting of the data.

Figure 4 shows the cosine of water contact angle θ on HMX 011, 010, and 110 surfaces for the water droplets containing 2000, 4000, and 8000 water molecules (from right to left). According to the modified Young's equation 1, extending these linear fits to the limit of infinitely large droplets (where $1/r_B = 0$) results in the cosine of macroscopic contact angles $cos\theta_\infty$. The extrapolated

macroscopic contact angles for water molecules on HMX 011, 010, and 110 surfaces are 69.98°, 60.82°, and 51.50°, respectively. These values are in excellent agreement with the experimental measurement by Yee at. el. [?] where water contact angle of 70°, 60°, and 50° are obtained for HMX 011, 010, and 110 surfaces, respectively. Previous studies have shown that water contact angle is a good indicator for surface polarity, with small contact angle for polar surface and large contact angle for apolar surface [20, 21]. The difference in water contact angle on HMX surfaces shows that their polarity is different, with strongest polarity for 110 surface and weakest polarity for 011. This difference could be partially attributed to the density of polar group ($-NO_2$) on the HMX surface. As shown by Cady et al., the 110 surface contains more NO_2 group than the 011 surface [22]. Previous experimental study has shown that under compressive loading twinning takes place on the 101 plane, cleavage in β-HMX takes place on the 011 plane [23], which could be explained by the lower polarity of the 011 surface of β-HMX (????).

According to equation 1, the slope of the fits in Figure 4 gives $-\frac{\tau}{\gamma_{LV}}$ and the values are -0.227 nm, -0.841 nm, and 0.289 nm for HMX surface 011, 010, and 110 respectively. Since the surface tension of water is $\gamma_{LV} = 0.072N/m$, the line tension is found to be 1.6344×10^{-11} J/m, 6.0552×10^{-11} J/m, and -2.0808×10^{-11} J/m. From equation 1, we know the effect of a positive line tension is to contract the droplet base and to increase the contact angle whereas a negative τ enhances wetting. Experiments directed toward clarifying these issues would be particularly welcome. (Do we need this paragraph?)

B. Adhesive force

Figure 5 (left) shows the free energy required to pull the Estane hard segments off from the HMX surfaces containing nitroplasticizer. These free energy profiles are not strictly linear for all of these surfaces due to the rigidity of the Estane hard segment. In particular, this deviation is larger for 010 surface, which could be attributed to both the rigidity of the hard segment and the roughness of the HMX 010 surface. As shown in Figure 6, the 010 face of HMX crystal has more variation as compared to 011 and 110 face. Figure 5 also shows linear fits to each set of free energy data points. Slopes of these linear fits give the forces need to detach the Estane, 84 pN, 96 pN, and 133 pN for HMX 011, 010, and 110 surfaces, respectively. Clearly, the detachment force increases with the increasing polarity of HMX surfaces. The force is strongest for polar 110 surface and weakest for less polar 011 surface.

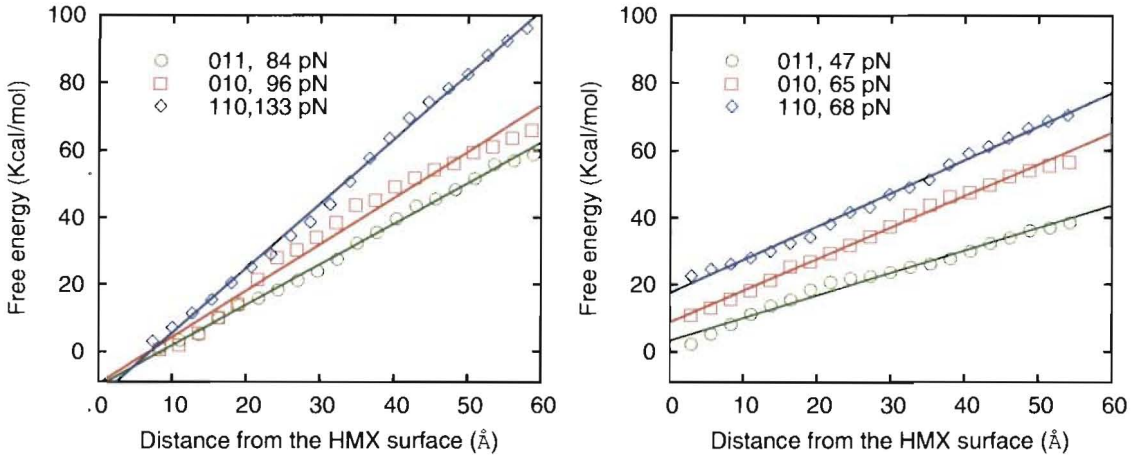

FIG. 5: Free energy as a function of distance between the first hard segment to the surfaces of HMX (dots). Linear fits of these free energy profiles are also shown (lines), with the slopes of these lines representing the forces required to pull off the Estane chain from the HMX surfaces. Left figure shows the results from the system with nitroplasticizer and right figure shows the results from the system without nitroplasticizer. For visual clarity, the free energy profiles are shifted by 10 Kcal/mol and 20 Kcal/mol for 010 and 110 surfaces, respectively.

The free energies and forces required to pull off Estane chain from HMX surfaces without nitroplasticizer are also shown in Figure 5 (right). Again, the detaching force increases with the increasing of HMX surface polarity, from 47 pN for 011 surface to 65 pN for 010 surface and 68 pN for 110 surface. Clearly, these detaching froces data indicate the HMX surface polarity dominates the adhesion interaction between Estane and HMX. Interesting, the detaching forces are systematically smaller than that of HMX surfaces with nitroplasticizer, indicating nitroplasticizer also play an important role in binding the HMX crystal with Estane binder. The energetic interactions between Estane, HMX and nitroplasticizer (if present in the system) are calculated for all HMX surface and and Estane detaching status. We found that the attraction between Estane and HMX are actually decreased with the present of nitroplasticizer, partially due to the competition of nitroplasticizer for favorable position on HMX surface. It is the attraction between Estane and nitroplasticizer that makes the Estane detaching forces larger. Since the surface structure are different for 011, 010, and 110 surface, the extent of nitroplasticizer in enhancing the adhesion between Estane and HMX surfaces is also different. This is confirmed from the difference of the detaching forces with and without nitroplasticizer on the HMX surfaces, namely, 37 pN for 011,

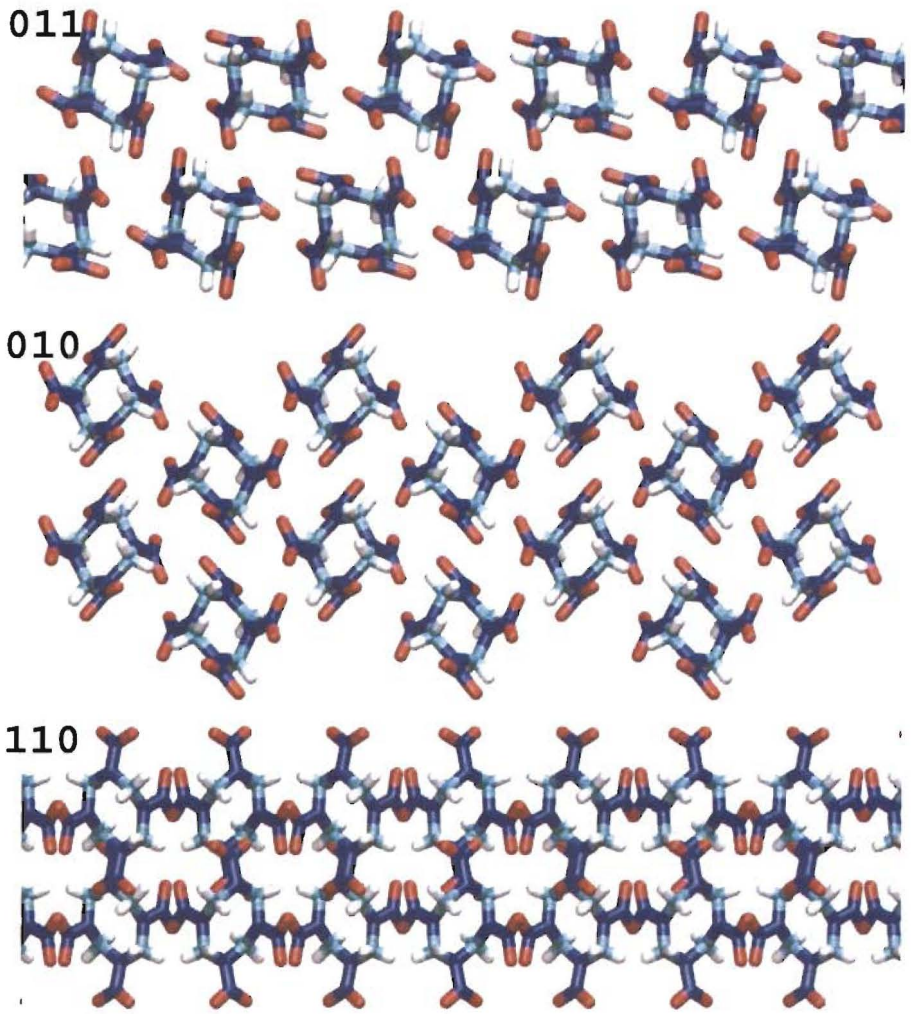

FIG. 6: Side view of the HMX crystal 011, 010, and 110 surface with oxygen in red, hydrogen in white, nitrogen in blue, and carbon in cyan

31 pN for 010, and 65 pN for 110.

IV. CONCLUSION

We have presented a systematic study of the surface properties of HMX crystal principle surfaces 011, 010, and 110. The contact angle of water droplet has served as a measure of the surface polarity. The macroscopic water contact angles extrapolated from the microscopic simulation results have excellent agreement with the experimental measurement. The results indicate the polarity of HMX surfaces increases from 011, to 010 to 110. The adhesion between these HMX

surfaces and the Estane binder with and without nitroplasticizer is also investigated. In both cases, the free energy and force of detaching Estane chain from the HMX surface increases with the surface polarity, indicating surface polarity dominates the adhesion interaction. The comparsion of the detaching forces with and without the present of nitroplasticizer shows that the nitroplasticizer also plays an important role in the binding of Estane and HMX surfaces. Although a great deal of work remains in order for us to fully understand HMX-Estane binder interface, the study reported here represents the first application of molecular modeling and simulation to interfaces found in PBX materials and the results have been encouraging. Our MD simulations and theoretical calculations of the multi-constituent composite material may provide some information and guidance for composite design.

Acknowledgments

This research was support by the LDRD-ER program (grant No. xxxxx) Los Alamos National Laboratory is operated by Los Alamos National Security, LLC, for the National Nuclear Security Administration of the U.S. Department of Energy under contract DE-AC52-06NA25396.

---

[1] T. RIVERA and M. L. MATUSZAK, JOURNAL OF COLLOID AND INTERFACE SCIENCE **93**, 105 (1983), ISSN 0021-9797.

[2] H. Kim, A. Lagutchev, and D. D. Dlott, Propellants, Explosives, Pyrotechnics **31**, 116 (2006), ISSN 0721-3115.

[3] L. Smilowitz, B. F. Henson, M. Greenfield, A. Sas, B. W. Asay, and P. M. Dickson, Journal of Chemical Physics **121**, 5550 (2004), ISSN 0021-9606.

[4] L. Smilowitz, B. F. Henson, B. W. Asay, and P. M. Dickson, Journal of Chemical Physics **117**, 3789 (2002), ISSN 0021-9606.

[5] C. K. Saw and C. M. Tarver, 13th Conference of the American Physical Society Topical Group on Shock Compression of Condensed Matter p. 1029 (2003).

[6] C. F. Macrae, P. R. Edgington, P. McCabe, E. Pidcock, G. P. Shields, R. Taylor, M. Towler, and J. van de Streek, Journal of Applied Crystallography **39**, 453 (2006), ISSN 0021-8898.

[7] G. D. Smith and R. K. Bharadwaj, JOURNAL OF PHYSICAL CHEMISTRY B **103**, 3570 (1999),

ISSN 1520-6106.

[8] G. D. Smith, D. Bedrov, O. Byutner, O. Borodin, C. Ayyagari, and T. D. Sewell, Journal of Physical Chemistry A **107**, 7552 (2003), ISSN 1089-5639.

[9] H. Davande, O. Borodin, G. D. Smith, and T. D. Sewell, JOURNAL OF ENERGETIC MATERIALS **23**, 205 (2005), ISSN 0737-0652.

[10] H. Davande, D. Bedrov, and G. D. Smith, JOURNAL OF ENERGETIC MATERIALS **26**, 115 (2008), ISSN 0737-0652.

[11] H. J. C. Berendsen, J. R. Grigera, and T. P. Straatsma, J. Phys. Chem. **91**, 6269 (1987).

[12] T. Darden, D. York, and L. Pedersen, J. Chem. Phys. **98**, 10089 (1993).

[13] J. P. Ryckaert, G. Ciccotti, and H. J. C. Berendsen, J. Comput. Phys. **23**, 327 (1977).

[14] H. J. C. Berendsen, J. P. M. Postma, W. F. van Gunsteren, A. DiNola, and J. R. Haak, J. Chem. Phys **81**, 3684 (1984).

[15] T. Werder, J. H. Walther, R. L. Jaffe, T. Halicioglu, and P. Koumoutsakos, Journal of Physical Chemistry B **107**, 1345 (2003), ISSN 1089-5647.

[16] N. Giovambattista, P. G. Debenedetti, and P. J. Rossky, Journal of Physical Chemistry B **111**, 9581 (2007), ISSN 1520-6106.

[17] J. Y. Wang, S. Betelu, and B. M. Law, PHYSICAL REVIEW E **63**, 031601 (2001), ISSN 1539-3755.

[18] S. KUMAR, J. M. ROSENBERG, D. BOUZIDA, R. H. SWENDSEN, and P. A. KOLLMAN, Journal of Computational Chemistry **16**, 1339 (1995), ISSN 0192-8651.

[19] B. ROUX, Computer Physics Communications **91**, 275 (1995), ISSN 0010-4655.

[20] P. G. de Gennes, Rev. Mod. Phys. **57**, 827 (1985).

[21] S. R. HOLMESFARLEY, C. D. BAIN, and G. M. WHITESIDES, Langmuir **4**, 921 (1988), ISSN 0743-7463.

[22] H. H. CADY, D. T. CROMER, and A. C. LARSON, ACTA CRYSTALLOGRAPHICA **16**, 617 (1963), ISSN 0108-7673.

[23] S. J. P. Palmer and J. E. Field, Proceedings of the Royal Society of London, Series A (Mathematical and Physical Sciences) **383**, 399 (1982), ISSN 0080-4630.